Electrochimica Acta 251 (2017) 651–659

Contents lists available at ScienceDirect

Electrochimica Acta

journal homepage: www.elsevier.com/locate/electacta

Electrodeposition of germanium-containing precursors for $Cu_2(Sn,Ge)S_3$ thin film solar cells

João C. Malaquias[a,1,*], Minxian Wu[a,1], Jiajia Lin[a], Erika V.C. Robert[b], Jeroen Sniekers[c], Koen Binnemans[c], Phillip J. Dale[b], Jan Fransaer[a]

[a] Department of Materials Engineering, KU Leuven, Kasteelpark Arenberg 44, B-3001 Leuven, Belgium
[b] Physics and Materials Science Research Unit, University of Luxembourg, 41, rue du Brill, L-4422, Belvaux, Luxembourg
[c] Department of Chemistry, KU Leuven, Celestijnenlaan 200F, B-3001 Leuven, Belgium

ARTICLE INFO

Article history:
Received 20 June 2017
Received in revised form 12 August 2017
Accepted 17 August 2017
Available online 25 August 2017

Keywords:
Electrochemistry
Photovoltaics
CTS
CTGS
Germanium

ABSTRACT

$Cu_2(Sn,Ge)S_3$ has recently emerged as an absorber layer for single junction thin film solar cells, already achieving power conversion efficiencies of up to 6.7%. Electrodeposition of metallic precursors and their subsequent annealing is an attractive synthesis method for such solar cell absorber layers, since it does not require vacuum conditions and little energy is consumed. The aqueous electrodeposition of metallic germanium based on current knowledge is limited to very thin layers, which do not provide the stoichiometric amount of material required for thick semiconductor layers. Therefore we introduce an electrodeposition method for the growth of germanium-containing precursors for $Cu_2(Sn,Ge)S_3$, using propylene-glycol-based electrolytes. These baths do not require additives, give rates of germanium electrodeposition higher than other plating baths and are cheap. The electrochemical behaviour of copper, tin and germanium in propylene glycol was studied and the corresponding deposits were characterised. Smooth and compact layers of each of the pure elements were deposited. Additionally, the co-electrodeposition of copper and germanium was studied as well and thin films containing the alloy Cu_3Ge and metallic copper were obtained. A constant [Cu]/[Ge] ratio of around 3 was found over a wide potential range, with a higher plating efficiency than that of pure germanium. For these reasons, copper and germanium were incorporated into the precursor via the referred co-deposition method. After thermal annealing in the presence of elemental sulphur, the semiconductor $Cu_2(Sn,Ge)S_3$ was successfully formed and it was incorporated in a working solar cell structure with efficiency of 0.7%

1. Introduction

Interest in the semiconductor $Cu_2ZnSn(S,Se)_4$ (kesterite) as a potential alternative absorber material for solar cells increased over the last decade, since this material consists of relatively abundant and cheap elements. However, development of solar cells based on kesterite has been slow, achieving a maximum efficiency of only 12.6% [1]. Cu_2SnS_3 is a *p*-type semiconductor just like kesterite, but contains one element less thus reducing the number of possible secondary phases and defects. An efficiency of 4.6% was recently achieved for solar cells based on this material [2]. Umehara et al. demonstrated a higher device efficiency of 6.0% by replacing some of the tin with germanium, to form $Cu_2(Sn,Ge)S_3$ (CTGS) [3]. The authors attributed the increased efficiency to the enrichment of grain boundaries with germanium, thus resulting in a local increase of the band gap [4]. Most recently, Umehara and co-workers achieved a new record efficiency of 6.7% by using an absorber layer with a graded band gap through the depth of the film [5]. Various physical growth methods have been applied for the growth of compounds in the CTGS material system. Umehara and co-workers co-sputtered Cu-Sn precursors and thermally annealed them in the presence of sulphur and GeS_2 [3,5]. For CGS solar cells Araki *et al.* deposited a Mo/Cu/Ge stack, with germanium being deposited via thermal evaporation and copper via e-beam evaporation [6]. Kim and co-workers co-evaporated Cu, Sn, Ge and Se [7]. Htay *et al.* sulphurised laminated copper, germanium and tin layers in a closed tube in order to study CTGS material properties as a function of the germanium content in the semiconductor [8]. Concerning wet chemical growth methods, a solvothermal route was employed by Peng *et al.*, who mixed solutions containing $GeCl_4$, $CuCl_2{\cdot}2H_2O$, $SnSO_4$ and sulphur powder in an autoclave and

* Corresponding author.
E-mail address: joaocmalaq.kul@gmail.com (J.C. Malaquias).
[1] These authors have contributed equally to this manuscript.

http://dx.doi.org/10.1016/j.electacta.2017.08.107
0013-4686/

heated the mixture to a high temperature in an oven [9]. Jin *et al.* synthesised a precursor containing copper and germanium for CGS-based solar cells by combustion of a solution containing copper(II) nitrate, citric acid, ammonia, nitric acid and germanium (IV) oxide [10]. The resulting powder was deposited on molybdenum using a doctor blade method and sulphurised. The authors reported a solar cell efficiency of 2.67%, being the highest for this material. Electrochemical methods were only used for the growth of CTS by electrodeposition of a metallic precursor and annealing (EDA), as shown by the works of Berg *et al.*, Robert *et al.* and Koike *and* co-workers [11–13]. It is not surprising that electrochemical processes have not yet been applied to the growth of germanium-containing precursors for CTGS solar cells, since hydrogen evolution has a low overpotential on germanium so that it cannot be efficiently electrodeposited from aqueous solutions [14]. A low hydrogen overpotential implies that gas evolution occurs extensively in parallel with the reduction of germanium(IV) and current efficiencies drop dramatically. Only ultrathin germanium layers contaminated by hydroxide and hydride species could be obtained, which is undesirable for photovoltaic applications. To avoid hydrogen evolution and electrodeposit pure germanium layers, ionic liquids have been used [15–19]. These works showed that despite being possible to electrodeposit germanium from ionic liquids, there were several issues: the germanium sources are poorly soluble in the ionic liquids, non-standard experimental setups had to be used to cope with the volatility of the most common germanium compounds and deposition rates are low under standard conditions. In another approach, Bartlett *et al.* electrodeposited amorphous germanium from liquid CH_3CN, CH_2F_2 and supercritical CH_2F_2 and CO_2, using $GeCl_4$ and $[NBu^n{}_4][GeCl_3]$ as germanium sources [20,21]. Albeit successful, this approach presents some drawbacks: on the one hand, the need of a high pressure cell, which increases the complexity of the experiment and decreases output. On the other hand, all the electrodeposited germanium layers contained impurities such as chlorine, which can be harmful to the performance of optoelectronic devices.

Another alternative is to use electrolytes based on organic solvents. Szekely electrodeposited germanium from propane-1,2-diol (here referred to as propylene glycol and abbreviated to PG) and ethane-1,2-diol (ethylene glycol) solutions containing $GeCl_4$ [22]. This author reported the deposition of thick and bright germanium layers from both electrolytes, but the process involving PG was considered better, since a graphite anode could be used thus avoiding the formation of precipitates in the solution. Nevertheless, the faradaic efficiency of the process was low (about 1%), since the best quality films were obtained when plating outside the electrochemical stability window of PG. Saitou and co-workers electrodeposited germanium from PG-containing $GeCl_4$ as well [23]. These authors reported the presence of Ge-H bonds in the film determined by infrared spectroscopy and stated that no bright deposits were obtained. The fact that Saitou *et al.* did not dry their PG solution, as opposed to Szekely, suggests it is essential to remove as much water as possible from this organic solvent. This literature survey shows that organic solvents are at this point the most sensible option when electrodepositing germanium for photovoltaic applications, since the layers exhibit high quality and deposition rates of 8 $\mu m.h^{-1}$ can be achieved [22]. Moreover, these solvents are much less expensive than ionic liquids and do not require special setups to electrodeposit germanium. In fact, Clauwaert *et al.* already used the method introduced by Szekely to incorporate for the first time a germanium layer into electrodeposited Mo/Cu-Zn/Sn stacked precursors for $Cu_2Zn(Sn, Ge)Se_4$-based solar cells [24].

Interestingly, alloys of germanium and copper can be electrodeposited from aqueous electrolytes as shown in the works of Fink and Joi [25,26]. These authors electrodeposited Cu-Ge thin films with constant [Cu]/[Ge] ratio of 3, forming the alloy Cu_3Ge. The electrodeposition of the intermetallic is easier than the deposition of pure germanium, due to the negative Gibbs free energy of the alloy and hence to a more positive redox potential [27]. This mechanism is generally referred to as Kroger's mechanism and is of the utmost importance when aiming for the electrodeposition of quality materials and with controlled chemical composition [27]. Still, the alkaline pH of those aqueous electrolytes may degrade the quality of the molybdenum back contact, since the Pourbaix diagram indicates that, even at negative potentials, this metal dissolves in solutions of such high pH [28]. Moreover, in recent work it was shown that oxygen is incorporated into Cu-Ge layers electrodeposited from aqueous electrolytes, which is undesirable for photovoltaic devices [29].

In this paper, we investigate the fabrication of CTGS solar cell absorber layers, using propylene-glycol-based electrolytes and thermal annealing. First we study the electrodeposition of copper, tin and germanium layers. Second, we study the co-deposition of copper and germanium and take advantage of the Kroger mechanism to grow layers containing Cu_3Ge to be used as precursors for CTGS solar cells.

2. Experimental

Electrolyte preparation and electrochemical work were performed inside an argon-filled glovebox (Glovebox Technologies Limited), with oxygen concentrations below 10 ppm and a moisture level below 1 ppm at all times. Prior to their use, $CuCl_2{\cdot}2H_2O$ (Alfa Aesar, 98%), $SnCl_2{\cdot}2H_2O$ (Alfa Aesar, 98%), NaCl (Merck) and $Na_2SO_4{\cdot}10H_2O$ (Acros Organics, 99%) were dried on a Schlenk line, under vacuum (p = 50 Pa) at 110 °C, during 24 hours. Propane-1,2-diol, hereafter referred to as propylene glycol (PG) (Sigma-Aldrich, 99.5%), was dried under identical conditions, but at room temperature. This solvent was further dried inside the glovebox by adding dried Na_2SO_4 to it, thus forming $Na_2SO_410H_2O$. This hydrated salt was then filtered, making the propylene glycol solution transparent and colourless. $GeCl_4$ (Umicore, 99.99%) was used as received. A Karl Fischer DL39 coulometer was used to determine the water content of the water content of PG and of the chloride compounds used. It was determined that after drying, the water content of PG was 0.06 wt%, that of $CuCl_2$ was 3.3 wt% and that of $SnCl_2$ was 8.7 wt%. The water content of NaCl could not be determined, since no dry solvent that can dissolve this salt was available. All electrolytes contained 0.50 M NaCl in order to increase the conductivity. A three-electrode cell was used for the electrochemical experiments. As counter electrode, a platinum foil was used in electrochemical experiments involving electrolytes containing only copper and tin, whilst for experiments where the electrolyte contained germanium, a graphite block was used. As reference electrode, a silver wire was first anodised in 0.1 M HCl (Analar Normapur, 37%) to form AgCl on its surface and then immersed in a propylene glycol solution containing 0.5 M NaCl. The set was enclosed in a fritted glass. Unless stated otherwise, for cyclic voltammetry (CV) and linear scan voltammetry (LSV) experiments, the working electrode was a molybdenum wire with a cross-section surface area of 2.8×10^{-5} m^2. An Ecochemie Autolab 302N potentiostat was used as power source in all experiments. CV experiments were recorded starting at open circuit potential and sweeping first in the cathodic direction. Electrodeposition was carried out on molybdenum coated sodalime glass substrates (SLG/Mo), with a surface area of approximately 4.0×10^{-4} m^2. Prior to electrodeposition, the substrates were etched during 5 min in NH_4OH (Merck, 25%), then rinsed with distilled water and absolute ethanol and dried. For the electrodeposition of tin, a rotating disk

electrode (ω = 150 rpm) was used to improve the uniformity of the deposit.

The resulting SLG/Mo/Cu(Sn,Ge) metallic precursors were thermally annealed in a tubular furnace to form the semiconductor. For the annealing process, all precursors were placed in a graphite box containing 100 mg of sulphur pellets (Alfa-Aesar, 99.999%) and 10 mg of GeS (Sigma-Aldrich, 99.99%), to minimise the loss of germanium. The graphite box was heated up to a temperature of 550 °C during 30 min, at a pressure of 100 Pa and in the presence of nitrogen gas. Prior to solar cell fabrication, the absorbers were etched in 5 wt. % KCN during 30 seconds to remove any $Cu_{2-x}S$ phases that may have formed.

The chemical composition of the thin films was determined using inductively coupled plasma optical emission spectroscopy (ICP-OES) and was performed using a Varian 720 ES spectrometer. Prior to the analysis, the thin films were dissolved in nitric acid (HNO_3, Sigma-Aldrich, 65%), to which a few drops of hydrogen peroxide (H_2O_2, Chem-Lab, 35%) were added. This method was preferred over the use of *aqua regia*, in order to avoid the formation of volatile germanium chloride species in solution, which would result in the underestimation of the germanium content in the layer. Scanning electron microscopy (SEM) was performed using a Philips XL 30 FEG microscope, to which an EDAX Genesis 4000 spectrometer was coupled for energy-dispersive X-ray spectroscopy (EDX). The SEM micrographs were taken using a 10 kV acceleration, whilst EDX was performed using a 20 kV acceleration. Grazing incidence X-ray diffraction (XRD) was performed either on a Seifert 3003 T/T diffractometer or on a Bruker Discover D8 diffractometer, using Cu Kα radiation with λ = 1.54056 Å and an incidence angle of 3°.

Solar cells were fabricated with the structure: Mo/CTGS/CdS/i-ZnO/Al:ZnO/Ni-Al contacts (cf. Figure 1). The CdS buffer layer (50 nm) was deposited by chemical bath deposition, both ZnO layers were sputtered (80 nm i-ZnO and 380 nm Al:ZnO) and the Ni-Al contacts were deposited by electron beam evaporation. Current-voltage measurements (j-V) were performed using a halogen light with an intensity of 1000 $W.m^{-2}$ in order to simulate the AM1.5 spectrum. The devices were then subjected to a post-fabrication annealing treatment, which resulted in an overall efficiency increase.

3. Results and Discussion

The results will be divided into four parts. In the first part, we describe the electrochemical behaviour of propylene glycol solutions containing $CuCl_2$, $GeCl_4$ or $SnCl_2$. In the second part, the chemical composition and microstructure of the resulting metallic precursors are characterised. In the third part, the co-electrodeposition of copper and germanium from propylene glycol solutions containing $CuCl_2$ and $GeCl_4$ is studied. That part focuses on both electrochemical and solid-state aspects. In the fourth part, the structural and electrical properties of the semiconductor and solar cells are characterised.

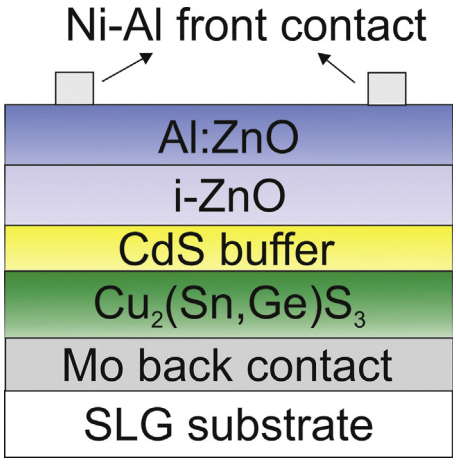

Figure 1. Schematic of the solar cell structure.

3.1. Electrochemical study of propylene glycol containing $CuCl_2$, $SnCl_2$ and $GeCl_4$ on molybdenum

Before studying the electrochemical behaviour of PG containing the elements to be electrodeposited, the electrochemical stability window of the blank electrolyte has to be assessed. In this work the electrolyte is considered to be stable within a potential range where the current density varies from -0.1 $A.dm^{-2}$ to 0.1 $A.dm^{-2}$, which is a commonly employed definition.

Figure 2a) depicts the LSV of PG containing 0.50 M NaCl on a molybdenum working electrode and shows that the electrolyte is stable between -1.7 V ≤ *E* ≤ 1.0 V. This observation implies that all electrodeposition processes should occur within the referred potential range, otherwise the energy efficiency of the process would decrease rapidly. Figure 2b) depicts the CV of PG containing 0.50 M NaCl and 0.10 M $CuCl_2$. On the forward scan, a reduction

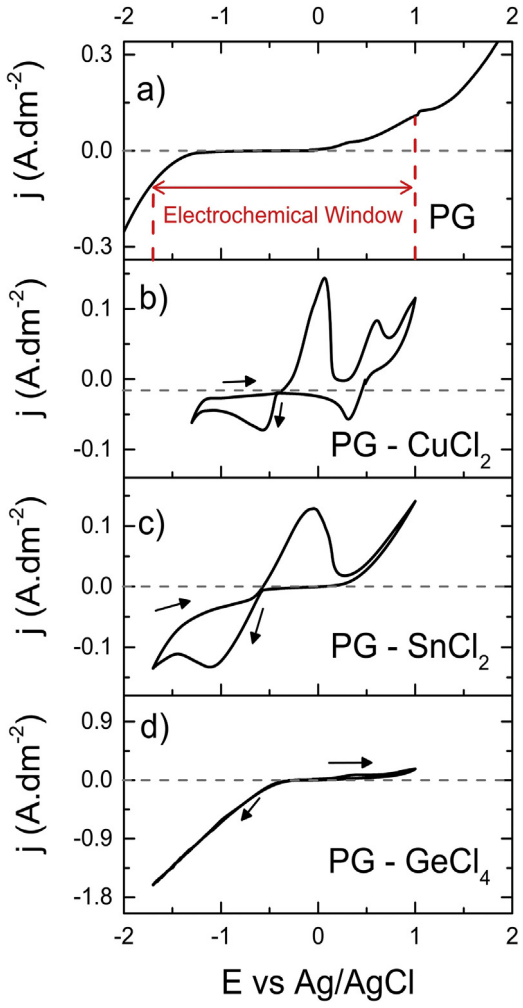

Figure 2. LSV of PG containing 0.50 M of NaCl on a molybdenum working electrode is depicted in a). CVs of PG containing 0.50 M NaCl and 0.10 M $CuCl_2$, or 0.05 M $SnCl_2$ or d) 0.45 M $GeCl_4$ on a molybdenum working electrode, are depicted in b), c) and d), respectively. All scans were recorded at room temperature with V_{scan} = 0.02 $V.s^{-1}$.

wave is recorded at $E = 0.5$ V, corresponding to the $Cu^{2+/+}$ reduction, since no deposition of material is observed. A second reduction onset is observed at $E = -0.4$ V, leading to the deposition of copper and thus corresponding to the reduction $Cu^{+/0}$. For potentials more negative than $E = -0.5$ V the system becomes diffusion-controlled, as suggested by the peak observed in the CV. On the reverse scan, an oxidation peak is observed at around $E = 0.0$ V, leading to the stripping of the copper deposited on the forward scan and thus corresponding to the oxidation $Cu^{0/+}$. Consequently, the second oxidation wave at $E = 0.6$ V corresponds to the oxidation $Cu^{+/2+}$. Figure 2c) depicts the CV of PG containing 0.50 M NaCl and 0.05 M $SnCl_2$ on a molybdenum working electrode. On the forward scan a reduction onset is observed at around $E = -0.6$ V, corresponding to the reduction $Sn^{2+/0}$ and leading to the deposition of metallic tin. For potentials more negative than $E = -1.0$ V, the system becomes diffusion-controlled. On the reverse scan, one oxidation peak is observed, corresponding to the stripping of the tin deposited on the forward scan. On the anodic side of the oxidation peak, a change in slope is observed. This change suggests that the oxidation may be occurring in two steps from Sn(0) to Sn(II) and then Sn(II) to Sn(IV). The standard reduction potential for $Sn^{2+/0}$ is -0.13 V (vs. SHE) and +0.15 V (vs. SHE) for $Sn^{4+/2+}$ [30]. Hence, the potential separation between the two reactions is of around 0.3 V and roughly corresponding to separation between the initial oxidation potential and the slope change. This observation may also explain why the anodic currents are slightly higher in the Sn CV than in the blank for $E > +0.5$ V. Figure 2d) depicts the CV of PG containing 0.45 M of $GeCl_4$ on a molybdenum working electrode. This CV depicts one cathodic current on the forward scan, which continuously increases as the potential is swept further in the negative direction. There are three factors contributing to this observation, which ultimately also make it impossible to accurately determine the reduction potential of germanium in PG. The first factor is related to the high concentration of germanium in the electrolyte and therefore no diffusion-limited regime is observed while the reduction $Ge^{4+/0}$ is occurring. The second factor is related to the low overpotential of hydrogen on germanium [14], implying that, as soon as a monolayer of germanium is formed on the electrode, a significant part of the cathodic current recorded is related to hydrogen evolution, despite the low water content of the organic solvent and of the chloride compounds used. We consider this hypothesis valid, since when electrolysing the pure liquid at current densities around -10 $A.dm^{-2}$ to study its cathodic decomposition products, the formation of a gas-phase species was observed. The fact that this gas species was too light to be identified by gas chromatography- mass spectrometry (GC-MS; experimental method in Appendix A) measurements, supports the hypothesis that hydrogen can be generated. The third factor is the electrochemical generation of germane (GeH_4), which has been shown to occur when immersing a germanium cathode into an electrolyte containing hydrogen [31]. Ultimately, most of the current flowing is related to the evolution of a gas-phase species, since it is described in literature that the faradaic efficiency of this deposition process is around 1% [22]. Moreover, these results imply that the electrochemical stability window of propylene glycol becomes narrower on a germanium working

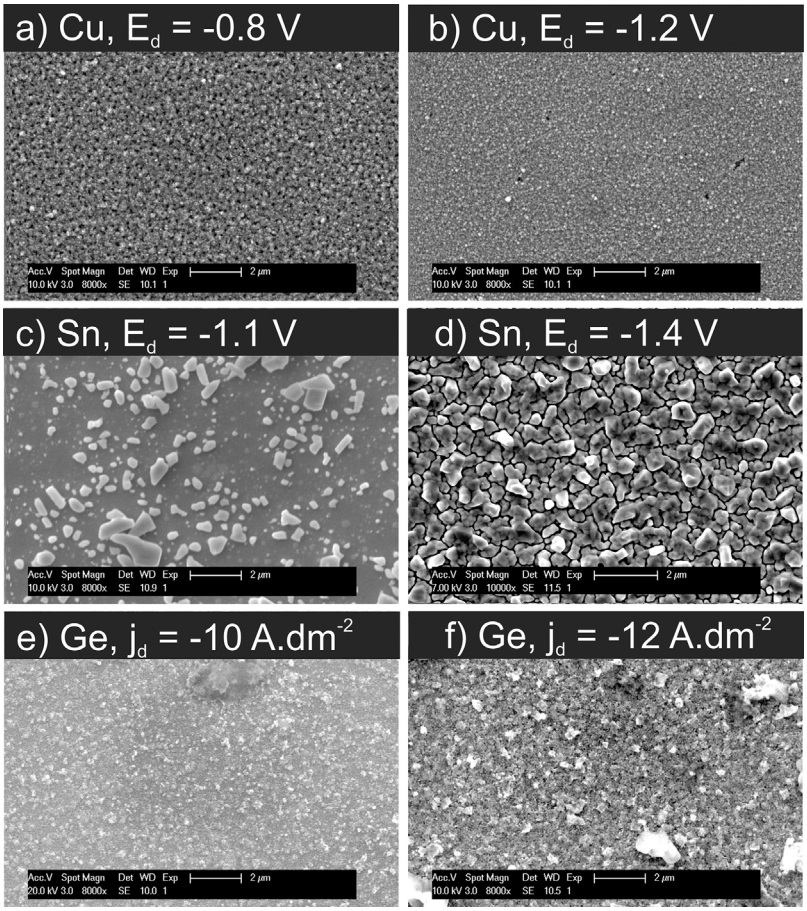

Figure 3. SEM top-view micrographs of Mo/Cu thin films electrodeposited at $E_d = -0.8$ V and $E_d = -1.2$ V from a PG solution containing 0.50 M NaCl and 0.10 M $CuCl_2$ are shown in a) and b), respectively. The micrographs in c) and d) are from Mo/Sn thin films electrodeposited from a PG solution containing 0.50 M NaCl and 0.05 M $SnCl_2$ at $E_d = -1.1$ V and $E_d = -1.4$ V, respectively. The surface of Mo/Ge thin films electrodeposited from a PG electrolyte containing 0.45 M $GeCl_4$ at $j = -10$ $A.dm^{-2}$ and $j = -12$ $A.dm^{-2}$ are depicted in e) and f), respectively.

electrode, which was confirmed by LSV and depicted in Figure A.1 of Appendix A. Still, after long periods of electrolysis at cathodic potentials, the formation of a layer on the working electrode is clearly observed. On the reverse scan of the CV in Figure 2d), no obvious anodic stripping peak is observed, suggesting that the process is irreversible. This observation is in accordance with previous studies, which showed that the electrodeposition of germanium from ionic liquids was irreversible [17,18]. Summing up, this section showed that the deposition of copper, tin and germanium onto molybdenum from propylene glycol is possible. Moreover, the redox potentials of copper and tin are close to each other, which would favour their simultaneous electrodeposition. Nevertheless, while the electrodeposition of copper and tin are efficient processes, since the ion reduction processes occur within the solvent window, the current efficiency of germanium deposition is very low due to the competing gas evolution processes.

3.2. Characterisation of the morphology of copper, tin and germanium thin films

The aim of this section is to assess the morphology of thin films electrodeposited at different potentials. Since the final precursor will consist of a stack of layers, the deposition of smooth and compact layers is preferred. Additionally, this morphology is advantageous for the final device performance as well, since it will facilitate charge transport and photon absorption, respectively.

Figure 3a) and b) show the top-view SEM micrographs for two Mo/Cu thin films deposited at E = -0.8 V and E = -1.2 V, respectively, with a thickness of 300 nm (as determined from the charge passed during deposition and the surface area of the film). Both micrographs depict a smooth and compact layer, with the grain size decreasing with higher overpotentials. This result is surprising, since in general the electrodeposition of copper from chloride-based electrolytes lead to the formation of rough and/or dendritic deposits in the absence of additives [32,33]. Additionally, EDX analysis revealed the deposition of pure copper and no chloride impurities. Figure 3c) and d) exhibit top-view SEM micrographs of Mo/Sn thin films deposited at E = -1.1 V and E = -1.4 V, respectively. The former micrograph depicts islands of tin scattered on the surface of the molybdenum, suggesting a low nucleation density. Regarding the latter micrograph, it shows a compact layer of tin fully covering the surface of the molybdenum substrate and with an apparent grain size of approximately 1 μm. Maltanava *et al.* electrodeposited tin onto copper from propylene glycol containing $SnCl_4 \cdot 5H_2O$ and obtained compact layers, with elongated crystals scattered on the surface [34]. The same authors reported that the morphology became smoother by adding boric acid to the electrolyte. The latter observation is contrary to what was observed in the work here reported, as no additive was needed to obtain smooth tin layers. EDX analysis showed that pure tin was electrodeposited. Figure 3e) and f) show top-view SEM micrographs of Mo/Ge thin films electrodeposited at j = -10 A.dm^{-2} and -12 A.dm^{-2}, respectively. As opposed to the potentiostatic deposition of copper and tin, the electrodeposition of germanium was carried out at a very negative constant current density, being clearly outside the stability window of the electrolyte. By proceeding in this manner, the deposition rate is significantly increased and kept constant, even though the current efficiency of the process is very low at around 1%. Moreover, variability issues in the layer properties brought by potentiostatic deposition outside the electrochemical stability window are avoided. Although the deposition process is occurring outside the stability window of the electrolyte, no obvious degradation of the liquid was observed and thin film quality remained identical to the films showed in Figure 3e) and f), even after plating dozens of layers from the same bath. Both layers are compact and smooth, with most of the surface being covered by sub-micron sized features. Nonetheless, there are a few micron-sized structures which are more prevalent on the film deposited at 12 A.dm^{-2}. Hence, performing deposition at the lower current density is more advantageous in terms of the morphology of the deposit. Macroscopically, these germanium layers are bright, in accordance with the results obtained by Szekely [22]. Similar to the tin and copper layers, no impurities were detected by EDX in the germanium layers. The electrodeposited germanium is only partly crystalline, since only the germanium 111 diffraction maximum is observed in the X-ray diffractogram (see Figure A.2 of Appendix A) and with low intensity. This observation is surprising, as electrodeposited germanium is in general amorphous [35]. The fact that smooth layers of all elements could be electrodeposited implies that any of the elements studied can be used as the first layer of a precursor stack and opens the possibility of studying different stacking orders.

3.3. Co-electrodeposition of copper and germanium from propylene glycol

In this section the simultaneous electrodeposition of copper and germanium from PG is studied. The main aim of this study is to obtain germanium-containing coatings with higher plating efficiency than that of pure germanium electrodeposition. This study follows on the works of Fink and Joi, who co-electrodeposited Cu_3Ge from a cyanide and tartrate based aqueous electrolytes, respectively [25,26]. Due to Kroger's mechanism, the authors reported faradaic efficiencies ranging from 25% to 95%. Hence, a similar effect should be observed when electrodepositing from PG.

Figure 4 depicts the CV of PG containing 0.45 M $GeCl_4$ and 0.05 M $CuCl_2$ on a molybdenum working electrode. The concentration of germanium in this electroplating bath is nearly 10 times higher than that of copper, in order to compensate for the low faradaic efficiency of germanium deposition verified in sections 3.1 and 3.2 and thus achieve the co-deposition of both elements. On the forward scan, a cathodic peak is recorded at around E = 0.4 V, which corresponds to the $Cu^{2+/+}$ reduction, as observed in Figure 2b). At E = -0.4 V a second cathodic current is recorded, which continuously increases as the potential is swept more negative, similar to the CV of PG containing $GeCl_4$ (cf. CV 2) in Figure 4)). This cathodic current leads to the deposition of material on the working electrode and is the sum of at least three redox reactions: 1) the reduction $Cu^{+/0}$, 2) the reduction $Ge^{4+/0}$ and 3) hydrogen evolution

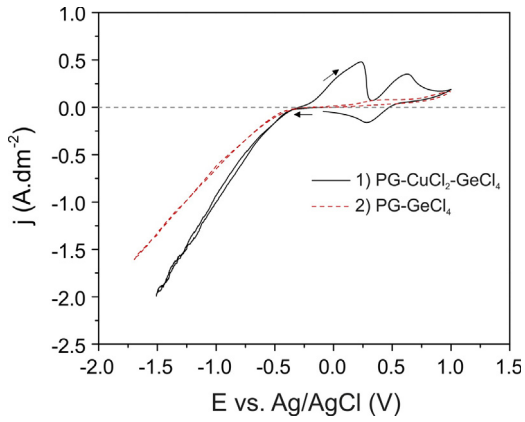

Figure 4. CV of PG containing 0.45 M $GeCl_4$ and 0.05 M $CuCl_2$ on a molybdenum working electrode is depicted in curve 1) (solid black line). The CV of PG containing 0.45 M $GeCl_4$ on a molybdenum working electrode is depicted in curve 2 (dashed red line). The scans were recorded at room temperature and with V_{scan} = 0.02 V.s^{-1}.

and/or formation of germane. On the reverse scan, a first oxidation peak is observed at around $E = 0.0$ V, corresponding to the stripping of the copper and germanium deposited on the forward scan. A second oxidation peak is recorded at $E = 0.5$ V and corresponds to the oxidation $Cu^{+/2+}$. Hence, the CV in discussion can be approximately described by the sum of CVs in Figure 1b) and 1d).

In order to confirm that the deposition of a Cu-Ge alloy is achieved, potentiostatic deposition was performed at potentials ranging from -2.4 V $\leq E \leq$ -0.6 V.

The chemical composition of the deposits, as determined by EDX and ICP-OES, are shown in Figure 5a). Interestingly, for deposition potentials more negative than $E = -0.8$ V, the [Cu]/[Ge] ratio is pinned to values around 3.0, suggesting the formation of Cu_3Ge. In these results, the ratios determined by ICP-OES are always higher than those determined by EDX, due to the loss of germanium during the dissolution of the sample. This loss probably occurs due to the formation of volatile germanium hydride compounds. The XRD diffractograms of the same thin films are depicted in Figure 5b) and show that Cu_3Ge (JCPDS Database 2011 89-1146) is formed at potentials more negative than $E = -0.8$ V, as expected.

Metallic copper (JCPDS Database 2011 04-0836) is detected as well, even on the layers deposited at the more negative potentials. This observation combined with the results on the chemical composition of the layers, suggest that there was not enough thermal energy available to promote alloying throughout the entire layer. If the copper detected would be in excess of the Cu_3Ge stoichiometry, then the [Cu]/[Ge] ratio of the deposits would be greater than 3. The fact that germanium is not detected is related to the poor crystallinity of this material, as previously discussed in section 3.2. Figure 6a)-e) depict exemplary top-view SEM micrographs of Mo/Cu-Ge thin films with [Cu]/[Ge] ratio around 3.0 and electrodeposited at different potentials. In general, all the layers display a compact morphology, but the layer deposited at $E = -0.8$ V (see Figure 6a) contains crystals scattered on its surface, giving it a rougher appearance. As the deposition potential becomes more negative, the predominance of these crystals decreases and the surface becomes smoother. This trend is apparent when comparing the micrographs of films deposited between -2.2 $\leq E_d \leq$ -0.8 V (Figure 6a) to d)). The thin film electrodeposited at $E_d = -2.4$ V (Figure 6e)) shows the smoothest surface. The corresponding cross-section image is depicted in Figure 6f), confirming that the layer is compact and that no voids are present. The plating efficiency (Φ) of this deposition process was determined by ICP-OES and the results are showed in Table 1.

As expected, the plating efficiency decreases as more negative potentials are employed, thus ranging from 27% for $E_d = -0.8$ V to 7% for $E_d = -2.4$ V. Although these values are still low, they represent an improvement of at least seven times, when compared to the electrodeposition of pure germanium. This improvement can be related to the fact that the Cu-Ge alloy is more stable than pure germanium, thus being more favourable to form. Ultimately, this implies that, per electron transferred, more material is electrodeposited from the Cu-Ge electroplating bath than from the germanium electrolyte.

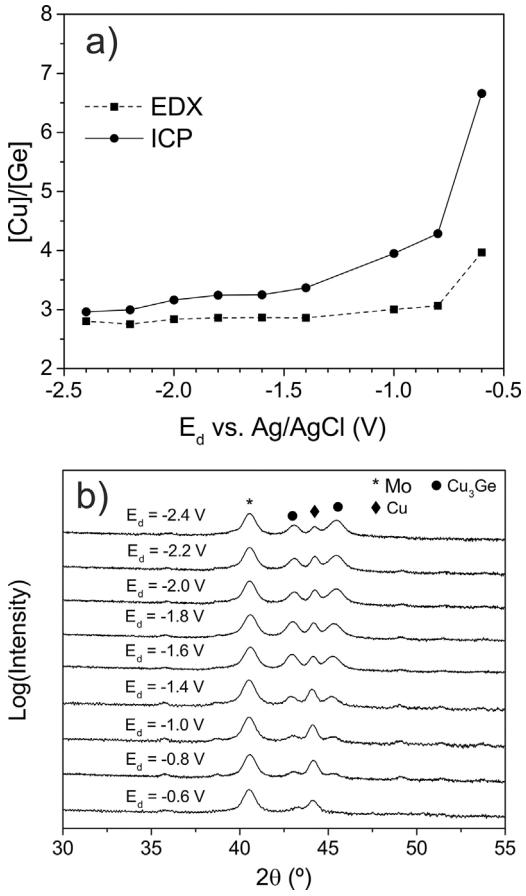

Figure 5. a)[Cu]/[Ge] ratio of electrodeposited Mo/Cu-Ge thin films. These ratios were measured by EDX and ICP-OES on thin films deposited from the same electrolyte and at deposition potentials ranging from -2.4 V $\leq E_d \leq$ -0.6 V. b) XRD of the same thin films.

3.4. Conversion to semiconductor and solar cell characterisation

In order to fabricate solar cells, precursor stacks containing copper, germanium and tin were thermally annealed in the presence of sulphur and germanium(II) sulphide, forming the $Cu_2(Sn,Ge)S_3$ semiconductor absorber layer. A Mo/Sn/Cu_3Ge precursor stack was plated, since this deposition method has a higher plating efficiency that a method involving the electrodeposition of a pure germanium layer. The precursor stack was plated with a chemical composition of [Cu]/([Ge+Sn]) = 2.0 and [Sn]/[Ge] = 0.5. Figure 7a) and b) show the top view and cross-section SEM micrographs of the absorber layer, respectively. The top view micrograph shows a compact layer, with a grain size below 1 μm. The cross-section micrograph depicts a layer with a thickness of around 1 μm and which is compact in its bulk. However, the interface between the absorber and molybdenum back contact exhibits voids, which are detrimental for charge carrier transport and thus for final solar cell efficiency.

After annealing, the chemical composition of the absorber was determined by EDX and ratios of [Cu]/([Ge+Sn]) = 1.9 and [Sn]/[Ge] = 0.2 were obtained, indicating that tin was lost during the annealing process. This loss occurs due to the evaporation of volatile SnS, formed during annealing [13,36]. Simultaneously, additional germanium was incorporated, due to the presence of germanium sulphide vapour in the atmosphere. Figure 7c) depicts the X-ray diffractogram of the absorber layer. Firstly, this diffractogram shows reflections related to the molybdenum substrate (JCPDS Database 2011 89-5023). Additionally, the diffraction peaks located at 2θ values around 29°, 34°, 48° and 54° are consistent with germanium-rich CTGS phase, since their angular positions are close to those of CGS (JCPDS Database 2011 88-0827). These results show that formation of the semiconductor was successful. After solar cell fabrication, a maximum device efficiency of 0.7% was obtained (V_{oc} = 186 mV and J_{sc} = -11.8 mA. cm^{-2}), as shown by the illuminated current-voltage curve depicted in Figure 7b). Although the efficiency is low, it is a first proof-of-principle for this synthesis routine. Interpreting the causes of the low efficiency from analysis of the *J-V* curve is difficult since the

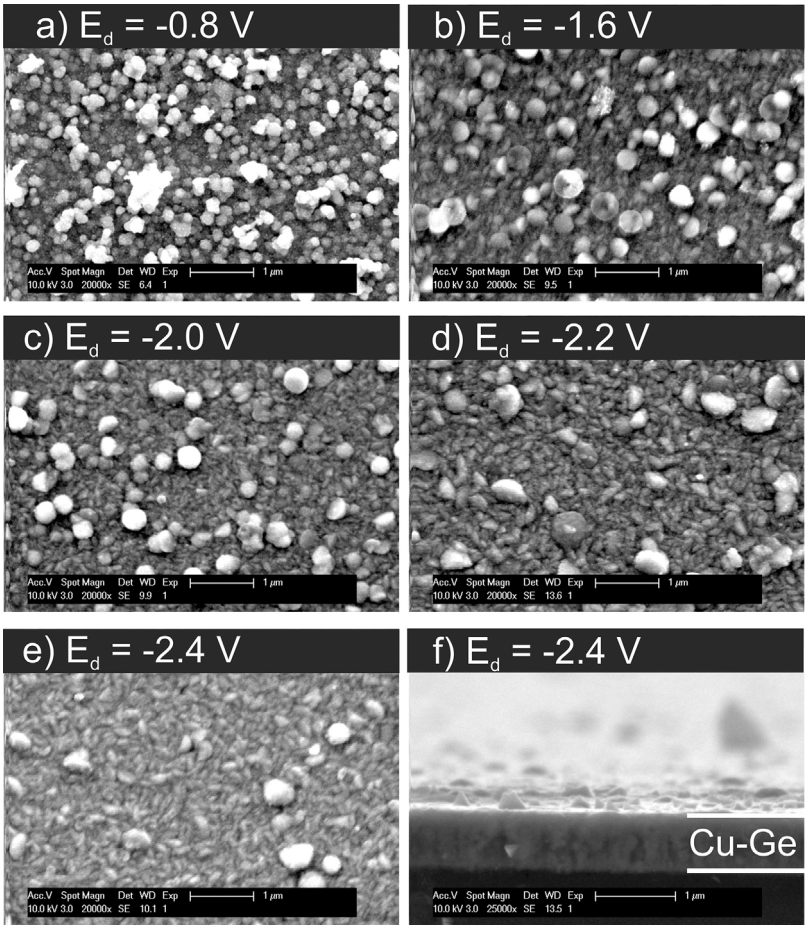

Figure 6. SEM top-view micrographs of Mo/Cu-Ge thin films electrodeposited at potentials ranging from -2.4 V ≤ E_d ≤ -0.6 V are depicted in a) – e). The cross-section micrograph of the Mo/Cu-Ge layer electrodeposited at E_d = -2.4 V is depicted in f).

Table 1
Plating efficiency (Φ) of the Cu-Ge electrodeposition process at potentials where thin films with [Cu]/[Ge] = 3.0 were obtained.

E_d vs. Ag/AgCl	Φ / %
−0.8	27
−1.0	19
−1.4	24
−1.6	13
−1.8	12
−2.0	9
−2.2	6
−2.4	7

data do not fit a simple model. A short circuit current of around 28.9 mA.cm^{-2} could have maximally been expected for a pure 1.5 eV band gap CGS device [37]. The absorption co-efficient of CGS is around 10^4 cm^{-1} [6] which would require a 2 micron thick absorber, i.e twice as thick than what was synthesized here, for complete absorption. Therefore the nearly three times lower current than expected can be partially explained by the thinness of the absorber layer. Still, this result shows that there is room for significant improvement.

4. Conclusion

This work introduced a straightforward and versatile electrodeposition an annealing method for the growth of CTGS absorber layers. The electrochemical behaviour of copper, tin and germanium in propylene glycol was studied. It was possible to efficiently electrodeposit compact and smooth layers of copper and tin onto molybdenum. The electrodeposition of germanium from the same organic solvent was possible as well. However, the current efficiency of the process was extremely low due to hydrogen evolution and the formation of germane. Still, compact and smooth germanium layers could be electrodeposited. To improve the current efficiency, the co-electrodeposition of copper and germanium was also studied and it was found that the CV of the mixture was approximately a sum of the CVs of the individual elements. Characterisation of the Mo/Cu-Ge thin films showed that the intermetallic Cu_3Ge was formed over a wide potential range, effectively pinning the [Cu]/[Ge] ratio of the deposit to values around 3. Moreover, compared to the electrodeposition of germanium, the plating efficiency of this process is more than seven times higher. A CTGS absorber layer was successfully grown and a solar cell with a maximum efficiency of 0.7% was prepared. This low value could be correlated to too thin an absorber layer and structural defects at the back electric contact/absorber interface. The growth route here introduced allows growing precursors with various stacking orders. Moreover, there is the underlying possibility to control the germanium content of the precursor and study its influence on the structural and optoelectronic properties of the final absorber layer.

Acknowledgements

The authors affiliated to the KU Leuven acknowledge financial support by the FWO- Flanders (research project G.0B9613.N) and

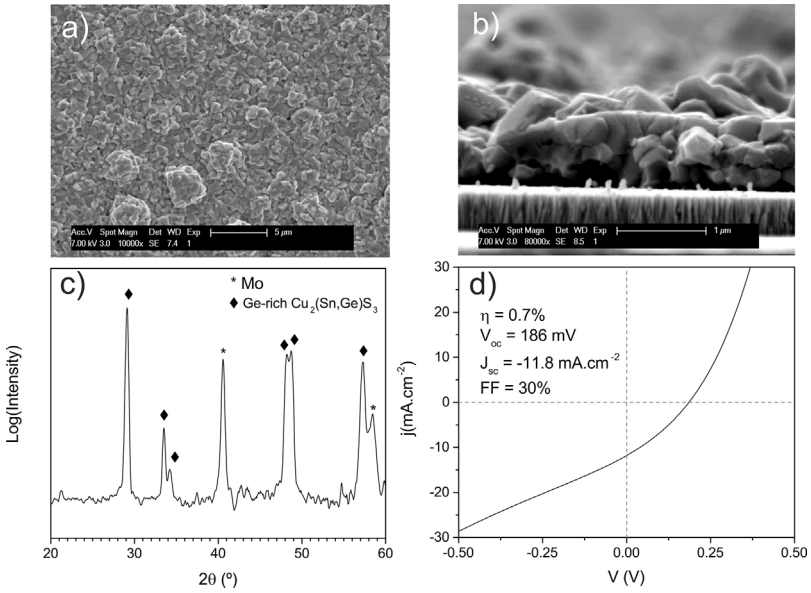

Figure 7. The top-view and cross-section SEM micrographs of the CTGS absorber layer are depicted in a) and b), respectively. The XRD and j-V curve of the absorber and solar cell are shown in c) and d), respectively.

KU Leuven (project IDO/12/006 IREBAT) and those affiliated to the University of Luxembourg thank the Fonds National de la Recherche for financial support through the grant C13/MS/5898466. Special acknowledgements to Dr Michele Melchiorre from the University of Luxembourg for the completion of the solar cell device from the absorber layer. The authors acknowledge Christine Wouters from the KU Leuven for the GC-MS measurement.

Appendix A. Supplementary data

Supplementary data associated with this article can be found, in the online version, at http://dx.doi.org/10.1016/j.electacta.2017.08.107.

References

[1] J. Kim, H. Hiroi, T.K. Todorov, O. Gunawan, M. Kuwahara, T. Gokmen, D. Nair, M. Hopstaken, B. Shin, Y.S. Lee, W. Wang, H. Sugimoto, D.B. Mitzi, High Efficiency $Cu_2ZnSn(S,Se)_4$ Solar Cells by Applying a Double In_2S_3/CdS Emitter, Advanced Materials 26 (2014) 7427–7431.
[2] N. Mitsuki, F. Junya, Y. Toshiyuki, I. Masanobu, Cu_2SnS_3 thin-film solar cells fabricated by sulfurization from NaF/Cu/Sn stacked precursor, Applied Physics Express 8 (2015) 042303.
[3] M. Umehara, Y. Takeda, T. Motohiro, T. Sakai, H. Awano, R. Maekawa, $Cu_2Sn_{1-x}Ge_xS_3$ (x = 0.17) Thin-Film Solar Cells with High Conversion Efficiency of 6.0%, Appl. Phys. Express 6 (2013) 045501.
[4] M. Umehara, Y. Takeda, K. Oh-Ishi, Y. Aoki, T. Motohiro, T. Sakai, R. Maekawa, Energy level diagram around Ge-rich grain boundaries in $Cu_2Sn_{1-x}Ge_xS_3$ (CTGS) thin-film solar cells, Solar Energy Materials and Solar Cells 134 (2015) 1–4.
[5] M. Umehara, S. Tajima, Y. Aoki, Y. Takeda, T. Motohiro, $Cu_2Sn_{1-x}Ge_xS_3$ solar cells fabricated with a graded bandgap structure, Applied Physics Express 9 (2016) 072301.
[6] H. Araki, K. Chino, K. Kimura, N. Aihara, K. Jimbo, H. Katagiri, Fabrication of Cu_2GeS_3-based thin film solar cells by sulfurization of Cu/Ge stacked precursors, Japanese Journal of Applied Physics 53 (2014) 05FW10.
[7] K.M. Kim, S. Kim, H. Tampo, H. Shibata, K. Matsubara, S. Niki, Narrow-bandgap $Cu_2Sn_{1-x}Ge_xSe_3$ thin film solar cells, Materials Letters 158 (2015) 205–207.
[8] M.T. Htay, T. Mandokoro, H. Seki, T. Sakaizawa, N. Momose, T. Taishi, Y. Hashimoto, K. Ito, Influence of Ge composition in the $Cu_2Sn_{1-x}Ge_xS_3$ thin-film photovoltaic absorber prepared by sulfurization of laminated metallic precursor, Solar Energy Materials and Solar Cells 140 (2015) 312–319.
[9] X. Peng, S. Zhang, Y. Xiang, Solvothermal synthesis of $Cu_2Zn(Sn_{1-x}Ge_x)S_4$ and $Cu_2(Sn_{1-x}Ge_x)S_3$ nanoparticles with tunable band gap energies, Journal of Alloys and Compounds 640 (2015) 75–81.
[10] X. Jin, L. Zhang, G. Jiang, W. Liu, C. Zhu, High open-circuit voltage of ternary Cu_2GeS_3 thin film solar cells from combustion synthesized Cu-Ge alloy, Solar Energy Materials and Solar Cells 160 (2017) 319–327.
[11] D.M. Berg, R. Djemour, L. Guetay, G. Zoppi, S. Siebentritt, P.J. Dale, Thin film solar cells based on the ternary compound Cu_2SnS_3, Thin Solid Films 520 (2012) 6291–6294.
[12] K. Junpei, C. Kotaro, A. Naoya, A. Hideaki, N. Ryota, J. Kazuo, K. Hironori, Cu_2SnS_3 Thin-Film Solar Cells from Electroplated Precursors, Japanese Journal of Applied Physics 51 (2012) 10NC34.
[13] E.V.C. Robert, J. de Wild, P.J. Dale, Reaction chemistry of group IV containing copper chalcogenide semiconductors Cu_2MX_3 (M = Sn, Ge and X = S, Se), Journal of Alloys and Compounds 695 (2017) 1307–1316.
[14] X. Liang, Y.-G. Kim, D.K. Gebergziabiher, J.L. Stickney, Aqueous Electrodeposition of Ge Monolayers, Langmuir 26 (2010) 2877–2884.
[15] F. Endres, Electrodeposition of a thin germanium film on gold from a room temperature ionic liquid, Physical Chemistry Chemical Physics 3 (2001) 3165–3174.
[16] F. Endres, S. Zein El Abedin, Nanoscale electrodeposition of germanium on Au (111) from an ionic liquid: an in situ STM study of phase formation Part II. Ge from $GeCl_4$, Physical Chemistry Chemical Physics 4 (2002) 1649–1657.
[17] F. Endres, S. Zein El Abedin, Nanoscale electrodeposition of germanium on Au (111) from an ionic liquid: an in situ STM study of phase formation Part I. Ge from $GeBr_4$, Physical Chemistry Chemical Physics 4 (2002) 1640–1648.
[18] M. Wu, N.R. Brooks, S. Schaltin, K. Binnemans, J. Fransaer, Electrodeposition of germanium from the ionic liquid 1-butyl-1-methylpyrrolidinium dicyanamide, Physical Chemistry Chemical Physics 15 (2013) 4955–4964.
[19] M. Wu, G. Vanhoutte, N.R. Brooks, K. Binnemans, J. Fransaer, Electrodeposition of germanium at elevated temperatures and pressures from ionic liquids, Physical Chemistry Chemical Physics 17 (2015) 12080–12089.
[20] C.Y. Cummings, P.N. Bartlett, D. Pugh, G. Reid, W. Levason, M.M. Hasan, A.L. Hector, J. Spencer, D.C. Smith, Supercritical Fluid Electrodeposition of Elemental Germanium onto Titanium Nitride Substrates, Journal of the Electrochemical Society 162 (2015) D619–D624.
[21] J. Ke, P.N. Bartlett, D. Cook, T.L. Easun, M.W. George, W. Levason, G. Reid, D. Smith, W.T. Su, W.J. Zhang, Electrodeposition of germanium from supercritical fluids, Physical Chemistry Chemical Physics 14 (2012) 1517–1528.
[22] G. Szekely, Electrodeposition of Germanium, Journal of The Electrochemical Society 98 (1951) 318–324.
[23] M. Saitou, K. Sakae, W. Oshikawa, Evaluation of crystalline germanium thin films electrodeposited on copper substrates from propylene glycol electrolyte, Surface and Coatings Technology 162 (2003) 101–105.
[24] K. Clauwaert, M. Goossens, J. De Wild, D. Colombara, P.J. Dale, K. Binnemans, E. Matthijs, J. Fransaer, Electrodeposition and selenization of brass/tin/germanium multilayers for $Cu_2Zn(Sn_{1-x}Ge_x)Se_4$ thin film photovoltaic devices, Electrochimica Acta 198 (2016) 104–114.
[25] A. Joi, R. Akolkar, U. Landau, Pulse plating of copper germanide, Applied Physics Letters 102 (2013) 134107.
[26] C.G. Fink, V.M. Dokras, Electrodeposition and Electrowinning of Germanium, Journal of The Electrochemical Society 95 (1949) 80–97.
[27] D. Lincot, J.F. Guillemoles, S. Taunier, D. Guimard, J. Sicx-Kurdi, A. Chaumont, O. Roussel, O. Ramdani, C. Hubert, J.P. Fauvarque, N. Bodereau, L. Parissi, P. Panheleux, P. Fanouillere, N. Naghavi, P.P. Grand, M. Benfarah, P. Mogensen, O.

Kerrec, Chalcopyrite thin film solar cells by electrodeposition, Solar Energy 77 (2004) 725–737.
[28] M. Pourbaix, Atlas of electrochemical equilibria in aqueous solutions, 2nd ed., National Association of Corrosion Engineers, Houston, 1974.
[29] F. Zhao, Y. Xu, M. Mibus, G. Zangari, The Induced Electrochemical Codeposition of Cu-Ge Alloy Films, Journal of The Electrochemical Society 164 (2017) D354–D361.
[30] A.J. Bard, L.R. Faulkner, Electrochemical Methods - Fundamentals and Applications, 2nd ed, John Wiley & Sons, Inc, New York, 2001.
[31] V.V. Turygin, M.K. Smirnov, N.N. Shalashova, A.V. Khudenko, S.V. Nikolashin, V. A. Fedorov, A.P. Tomilov, Electrochemical preparation of germane, Inorganic Materials 44 (2008) 1081–1085.
[32] Y.L. Kao, K.C. Li, G.C. Tu, C.A. Huang, Microstructural Study of the Effect of Chloride Ion on Electroplating of Copper in Cupric Sulfate-Sulfuric Acid Bath, Journal of The Electrochemical Society 152 (2005) C605–C611.
[33] M. Schlesinger, M. Paunovic, Modern Electroplating, 5th ed, John Wiley and Sons, Inc, New Jersey, 2010.
[34] H.M. Maltanava, T.N. Vorobyova, O.N. Vrublevskaya, Electrodeposition of tin coatings from ethylene glycol and propylene glycol electrolytes, Surface and Coatings Technology 254 (2014) 388–397.
[35] F. Martineau, K. Namur, J. Mallet, F. Delavoie, F. Endres, M. Troyon, M. Molinari, Electrodeposition at room temperature of amorphous silicon and germanium nanowires in ionic liquid, IOP Conference Series: Materials Science and Engineering 6 (2009) 012012.
[36] A. Weber, R. Mainz, H.W. Schock, On the Sn loss from thin films of the material system Cu–Zn–Sn–S in high vacuum, Journal of Applied Physics 107 (2010) 013516.
[37] A.J. McEvoy, L. Castañer, T. Markvart, Practical Handbook of Photovoltaics: Fundamentals and Applications, Second ed., Academic Press, Boston, 2012.